Available online at www.sciencedirect.com

SCIENCE DIRECT®

Magnetic Resonance Imaging 22 (2004) 1211–1221

MAGNETIC RESONANCE IMAGING

Geometric distortion in clinical MRI systems Part I: evaluation using a 3D phantom

Deming Wang[a,*], Wendy Strugnell[b], Gary Cowin[a], David M. Doddrell[a], Richard Slaughter[b]

[a]*Centre for Magnetic Resonance, The University of Queensland, St. Lucia, QLD 4072, Australia*
[b]*Cardiovascular MRI Research Centre, The Prince Charles Hospital, Chermside, QLD 4032, Australia*

Received 28 July 2004; accepted 1 August 2004

Abstract

Recently, a 3D phantom that can provide a comprehensive and accurate measurement of the geometric distortion in MRI has been developed. Using this phantom, a full assessment of the geometric distortion in a number of clinical MRI systems (GE and Siemens) has been carried out and detailed results are presented in this paper. As expected, the main source of geometric distortion in modern superconducting MRI systems arises from the gradient field nonlinearity. Significantly large distortions with maximum absolute geometric errors ranged between 10 and 25 mm within a volume of $240\times240\times240$ mm^3 were observed when imaging with the new generation of gradient systems that employs shorter coils. By comparison, the geometric distortion was much less in the older-generation gradient systems. With the vendor's correction method, the geometric distortion measured was significantly reduced but only within the plane in which these 2D correction methods were applied. Distortion along the axis normal to the plane was, as expected, virtually unchanged. Two-dimensional correction methods are a convenient approach and in principle they are the only methods that can be applied to correct geometric distortion in a single slice or in multiple noncontiguous slices. However, these methods only provide an incomplete solution to the problem and their value can be significantly reduced if the distortion along the normal of the correction plane is not small.

Keywords: Geometric distortion; Comprehensive assessment; Vendor's correction method; MRI; 3D phantom

1. Introduction

Geometric distortion in MRI can arise from a variety of sources. Apart from the tissue-dependent chemical shift and susceptibility differences, the major hardware-related sources contributing to geometric distortion in MRI are gradient field nonlinearity and the static field inhomogeneity. In the superconducting MRI systems equipped with sophisticated shimming coils, the geometric distortion due to the static field inhomogeneity can be expected to be small when compared with that arising from the gradient field nonlinearity. For example, the shimming technologies that have been developed in recent years now easily allow the field homogeneity inside the diameter spherical volume (DSV) to be maintained within a few hertz at a proton frequency of 63.87 MHz (1.5T). A field inhomogeneity of 10–15 Hz would only cause a maximum geometric error of less than 0.2 mm in the presence of a gradient of 2 mT/m. By comparison, the geometric distortion arising from the gradient field nonlinearity can be much larger and can cause serious concerns in certain MRI applications where high accuracy and precision are required.

The gradient field nonlinearity has become more of an issue in the new generation of gradient systems that are characterized by fast slew rates (short gradient rise times). In the design of the new generation of the gradient systems, gradient designers employ short gradient coils. As a consequence, the gradient field nonlinearity has been compromised. The problem of increased gradient field nonlinearity in the new generation of gradient systems has recently begun to receive attention, for example, with regard to its effect on diffusion-weighted MRI [1,2] and on phase contrast MRI [3,4].

This problem of gradient field nonlinearity became a consideration when trying to expand our long-running MRI volumetric study on brain atrophy due to Alzheimer's disease and normal aging [5–7] when employing newly

* Corresponding author. Tel.: +61 7 33654100; fax: +61 7 33653833.
E-mail address: deming@cmr.uq.edu.au (D. Wang).

0730-725X/$ – see front matter © 2004 Elsevier Inc. All rights reserved.
doi:10.1016/j.mri.2004.08.012

acquired Siemens Sonata 1.5-T MRI systems. Motivated by the lack of a satisfactory method for measuring geometric distortion in three dimensions, a novel 3D phantom-based technique was developed that provides a comprehensive and accurate measurement of the geometric distortion in MRI due to gradient field nonlinearity and static field inhomogeneity [8]. As this technique can provide unprecedented detail and accuracy of the geometric distortion in MRI, we have measured the geometric distortion in a range of clinical MRI systems to which we have access. These include systems equipped with gradient systems of varied length-to-diameter ratios. In addition, we have evaluated geometric distortion both with and without vendors' correction methods in order to evaluate the effectiveness as well as to demonstrate the shortfall of these correction methods. We report the findings in this paper (Part I). In the following paper (Part II), we will present results using a correction method that has been developed based on the phantom-mapped distortion data.

The present study makes no attempt to accentuate any comparison between different MRI systems in terms of the geometric distortion, rather it is aimed to give a comprehensive assessment of the geometric distortion in each individual MRI system, or more precisely, each gradient system. It is hoped that the information provided in the present study can act as a useful benchmark concerning the use of a particular type of MRI system for certain applications in which high precision and accuracy are of concern. Geometric distortion due to gradient field nonlinearity is always present in any MRI system. The gradient systems in MRI are often designed to meet certain specifications. The two key performance indexes, gradient field linearity and slew rate associated with a MRI gradient system, are competing factors and in principle they cannot "perform equally well" in any given gradient system. In gradient design, a compromise in gradient linearity is unavoidable if the required slew rate is to be achieved and this appears to be the case in the design of the new generation of the MRI gradient systems that have the principal design criteria of speed.

2. Method

2.1. The 3D phantom

The geometric distortion was measured using a recently developed phantom-based technique [8]. A novel feature of this technique is the use of a 3D phantom in which the control point positions (the markers) are defined along all three orthogonal axes. This was achieved by using a concept that a point in 3D space can be defined by using three orthogonal planes. This novel approach overcomes the shortfall of previously developed 2D geometric MRI phantoms in which only two coordinates of the control points in the imaging plane are defined and the coordinate along the axis normal to the imaging plane is undefined, and as a consequence, this coordinate is unmeasurable [9–16]. A phantom based on the new design and built to fit into the body coil in clinical MRI scanners contained an array of 10,830 (19×19×30) points spanning an effective volume of 257.04×259.02×261.0 mm^3 (with intervals of 14.28, 14.39 and 9.00 mm along the respective x-, y- and z-axes). For more details of this phantom, see Ref. [8].

2.2. Assessment of geometric distortion

Geometric distortion in three dimensions can be characterized by the positional deviations (geometric errors)

$$\mathrm{d}x(x,y,z) = x'(x,y,z) - x$$

$$\mathrm{d}y(x,y,z) = y'(x,y,z) - y$$

$$\mathrm{d}z(x,y,z) = z'(x,y,z) - z$$

$$\mathrm{d}r(x,y,z) = \sqrt{\mathrm{d}x^2 + \mathrm{d}y^2 + \mathrm{d}z^2}$$

where $x'(x,y,z)$, $y'(x,y,z)$ and $z'(x,y,z)$ are the coordinates in the distorted space (the image space) and x, y and z are the corresponding coordinates in the undistorted space. In the phantom-based measurement, the geometric distortion is mapped through the correspondence of the control point positions between the distorted image space and their true positions defined by the geometry of the phantom (undistorted space). In the present work, this correspondence can be described as follows

$$\mathrm{d}x_{ijk} = x'_{ijk} - x_{ijk}$$

$$\mathrm{d}y_{ijk} = y'_{ijk} - y_{ijk}$$

$$\mathrm{d}z_{ijk} = z'_{ijk} - z_{ijk}$$

$$\mathrm{d}r_{ijk} = \sqrt{\left(\mathrm{d}x_{ijk}\right)^2 + \left(\mathrm{d}y_{ijk}\right)^2 + \left(\mathrm{d}z_{ijk}\right)^2}$$

$$(i = 1\ldots19; j = 1\ldots19; k = 1\ldots30)$$

where x_{ijk}, y_{ijk} and z_{ijk} are the coordinates of the control points defined by the geometry of the phantom, and x'_{ijk}, y'_{ijk}, and z'_{ijk} are the corresponding coordinates of the control points measured in the distorted images of the phantom. Given the geometric distortion measured at the control points, the geometric distortion at any other point within the effective volume of the phantom can be approximated by a 3D interpolation method. In the present study, we simply used the trilinear interpolation method for calculating the positional deviations for any point other than the control points within the effective volume of the phantom.

In this study, the geometric distortion was assessed for two specific volumes of interest (VOI). The first VOI studied was a cube having a volume of 240×240×240 mm^3. This VOI is denoted as $VOI_c(240)$. The second VOI studied was a sphere with a radius of 95 mm and it is

denoted as $VOI_s(95)$. These two VOIs are considered to be representative for body- and neuro-imaging applications, respectively. Both VOIs have their centers coinciding with the isocenter of the magnet. The *x*-, *y*- and *z*-axes are taken, respectively, along the left-to-right, anterior-to-posterior and the head-to-foot directions. The origin of the coordinate axis system is also taken to be at the isocenter of the magnet.

The following parameters were used to characterize the geometric distortion:

1. maximum absolute deviations within axial planes (the *xy* plane) at a set of evenly sampled locations along the *z*-axis within the cubic VOI;
2. maximum absolute deviations on the surface of spheres at a set of sampled radii within the spherical VOI.
3. the mean (μ), standard deviation (σ) and maximum absolute deviations (max) within the cubic VOI;
4. the mean, standard deviation and maximum absolute deviations within the spherical VOI.

These are some of the parameters used in a comprehensive characterization scheme recently developed for assessment of geometric distortion in MRI [17]. Comprehensive sampling schemes have been developed for obtaining these statistical and maximum absolute deviations [17]. In brief, for the specified cubic VOI and the planes, sampling was made along the three axes with the same sampling interval of 5 mm. For the spherical VOI, a special sampling scheme that can give the most homogeneous sampling within a sphere was used. The use of these sampling methods ensures that the boundary surfaces of the VOIs are properly represented. More details about these sampling schemes have been given elsewhere [17].

2.3. Image processing

A key aspect in the phantom-based technique is the development of a fully automated and extremely robust algorithm for measuring the control point positions in the MR images of the phantom. The details of this algorithm have been given previously [8]. In brief, this algorithm makes the use of image edge features for defining the positions of the planes from which the coordinates of the control points are derived. In doing so, it employs a number of 3D image processing tools including the use of extended 3D Prewitt edge detectors [18]. In addition, the first moments are used that allow the control point positions to be measured with subvoxel accuracy. Typically, the coordinates of the control points can be measured with an average error between 0.1 and 0.2 mm, which is only a fraction of the voxel's dimensions of the phantom images.

2.4. MRI systems and MR acquisition protocols

Four 1.5-T MRI systems were investigated in the present study: a Siemens Sonata, a Siemens Quantum, a GE Signa EchoSpeed Plus equipped with a Body Resonance Module (BRM) gradient set and a GE Signa TwinSpeed which is equipped with two sets of gradient coils, TRM (Twin Resonance Module) Zoom and Whole. The phantom images acquired on the Siemens Sonata and Quantum systems used the same 3D imaging sequence, coded as *t1_Vibe_fs_tra* by Siemens. The following imaging parameter values were used: TE=4.50 ms, TR=10 ms, flip angle 12°, receiver bandwidth ±16.6 kHz, FOV=333.0×333.0 mm, 256 slices, slice thickness 1.3 mm, slice gap 0 mm, acquisition matrix 256×256. The corresponding voxel's dimensions were 1.305×1.305×1.300 mm. The phantom images acquired on the GE TwinSpeed and EchoSpeed Plus systems used a spin echo sequence, designated by GE as axial T1 FSE-XL, with the following imaging parameters: TE=10.1 ms, TR=640 ms, echo train length 2, flip angle 90°, receiver bandwidth ± 25 kHz, FOV 330.0×330.0 mm, 240 slices, slice thickness 1.3 mm, slice gap 0 mm, acquisition matrix 256×256. The corresponding voxel's dimensions were 1.289×1.289×1.300 mm.

All the phantom images were acquired using the system's body coil. Because of the relatively low sensitivity of this coil, its large spatial variability in signal intensity and the relatively small voxel size (~2.2 mm^3) employed in the acquisition of the phantom images, averages were necessary in order to achieve a reasonable signal-to-noise ratio (SNR) to ensure a successful extraction of the control point positions in the entire imaging volume. In the acquisition of the phantom images, between two and six averages were used. The use of different averages in the acquisition was partly to create a range of phantom images with different SNR levels to provide a further test of the robustness of this recently developed phantom-based technique [8].

For the Siemens systems, the 3D phantom could be easily positioned with its geometric center near the systems' isocenter. For the GE systems, due to the restricted space along the vertical axis (relatively high bed position), the phantom's geometric center was ~25 mm away from the isocenter along the vertical axis (*y*). The cubic VOI used for assessing the geometric distortion in the GE systems was slightly modified along the *y*-axis and the following size {(−120,120), (−95,120), (−120,120)} was used.

3. Results

In Fig. 1, a sequence of axial slices of the phantom MR image between *z*=92.3 and 98.8 mm is shown in the top row. Apart from the obviously visible distortions in the slice plane (the *xy* plane), the geometric distortion along the *z*-axis (normal to the slice plane) is also present by showing a characteristic distortion pattern arising from the gradient field nonlinearity of a typical *Z* gradient coil, the so-called potato chip warping. The originally flat surface of a grid panel is now warped and becomes spherically "shaped" as indicated by the circles shown in the successive slices with decreasing radius. The extracted positions of the control

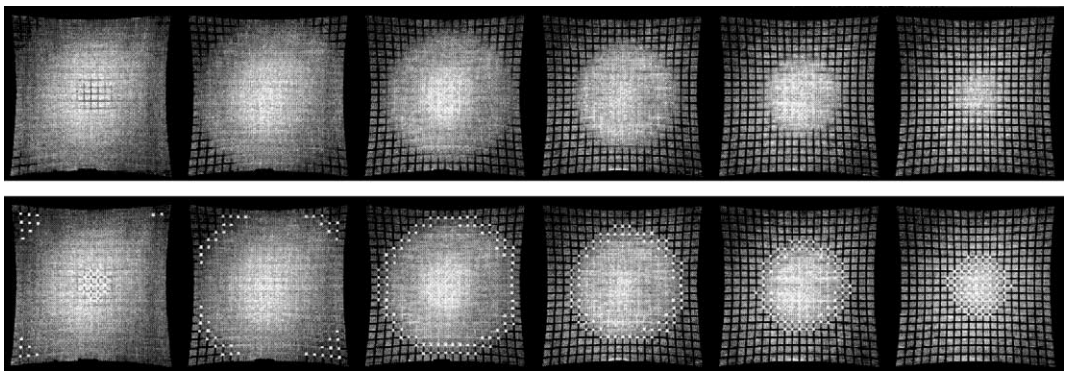

Fig. 1. A sequence of axial slices of the phantom MR image that traverse the surface of a grid panel of the phantom (top row), with the extracted control points (marked as squares) overlaid on the original images (bottom row).

points on the surface of this particular grid panel marked as white squares are overlaid on the original images (the bottom row). As shown, the entire warped image of the flat panel surface extends over six slices along the z-axis. This corresponds to a 6.5-mm positional shift along the z-axis. In fact, the control points marked in the center of the first slice were from a neighboring panel surface, which is 9 mm away from those appearing on the corners. In the method used in the present study, it is the differences between these control point positions measured in the distorted images along all three orthogonal axes and their true positions defined by the geometry of the 3D phantom that form a detailed assessment of the geometric distortion. In the following discussion, the geometric distortion is assessed in each of the MRI systems that formed the subject of this study.

3.1. Siemens Sonata

The results of the maximum absolute deviations of the geometric distortion measured in the axial planes for the Sonata system are shown in Fig. 2a (no correction) and Fig. 2b (with vendor's correction applied in the xy plane). The geometric distortion for the Sonata system with no correction is relatively large with the maximum absolute deviations of 10–11 mm occurring in slices at $z = \pm 120$ mm. This represents a deviation of 8–9% in relative terms. Clearly, the gradient field nonlinearity along both +z and $-z$

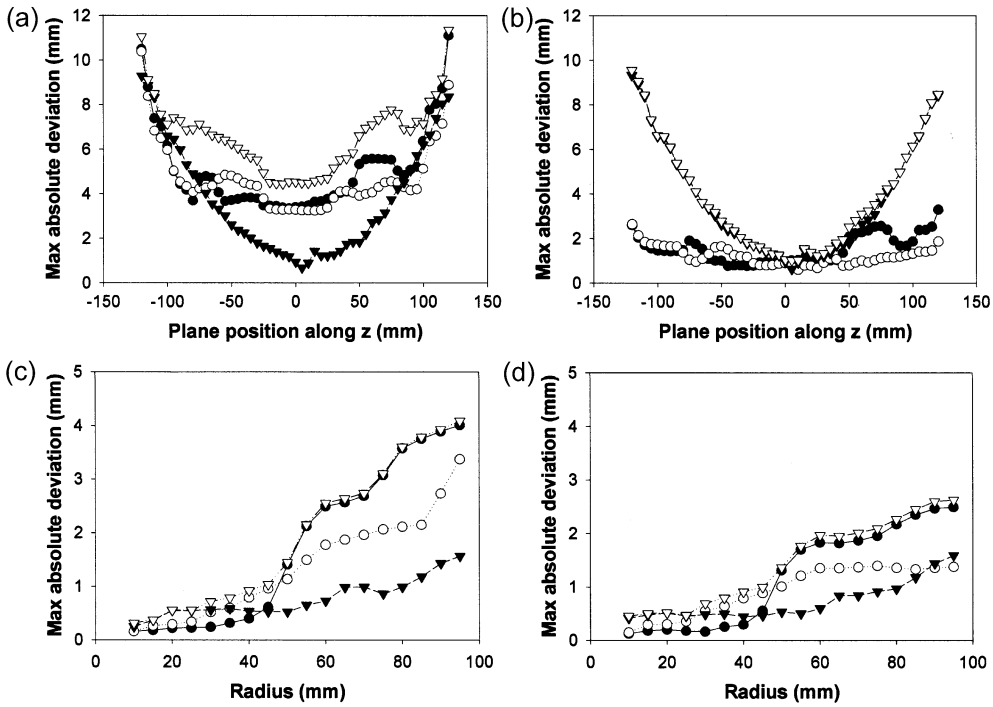

Fig. 2. The maximum absolute deviations (●, $|dx|_{max}$; ○, $|dy|_{max}$; ▼, $|dz|_{max}$;▽, dr_{max}) of the geometric distortion measured in a Siemens Sonata 1.5-T MRI system: (a) in axial planes on images acquired with no vendor's correction; (b) with vendor's correction applied in the xy plane; (c) on surface of spheres of different radius (no correction); (d) on surface of spheres of different radius (with correction).

Table 1
Summary of the statistical data (μ, σ, max) of the absolute deviations along x-, y- and z-axes and in the positional displacement (r) measured within a cubic VOI ($VOI_c(240)$: {(−120,120), (−120,120), (−120,120)}) and a spherical VOI ($VOI_s(95)$; R=95 mm) in a 1.5-T Siemens Sonata system

VOI	Vendor's correction	Direction	μ (mm)	σ	max (mm)
$VOI_c(240)$	No	x	1.76	1.87	11.1
		y	1.50	1.60	10.4
		z	1.20	1.18	9.3
		r	2.98	2.32	11.4
	Yes	x	0.69	0.61	3.3
		y	0.46	0.40	2.6
		z	1.20	1.19	9.3
		r	1.65	1.16	9.6
$VOI_s(95)$	No	x	0.51	0.70	4.0
		y	0.47	0.47	3.4
		z	0.29	0.24	1.6
		r	0.88	0.75	4.1
	Yes	x	0.41	0.50	2.5
		y	0.33	0.29	1.4
		z	0.29	0.24	1.6
		r	0.70	0.50	2.6

axes becomes considerably worse further away from the isocenter. In the central portion of the VOI ($|z|\leq 100$ mm), the maximum absolute deviations are ~6 mm. With the vendor's correction method applied in the xy plane, the distortion along the x and y in the entire VOI was significantly reduced with the maximum absolute deviations being about 2 mm or less, except in those slices at the edges of the VOI ($z=\pm 120$ mm) where the maximum absolute deviations were still large. As expected, the vendor's 2D correction method did not correct for any distortion along the axis normal to the correction plane (the z-axis). In Fig. 2c and d, the maximum absolute deviations measured on the surface of the spheres with different radii are shown without and with the vendor's correction, respectively. Before correction (Fig. 2c), the maximum absolute deviations were approximately 1 mm within the sphere of $r=50$ mm and the distortion increased quite dramatically as the radius increased from 50 to 95 mm. With the correction applied in the xy plane, the maximum absolute deviations were reduced as shown in Fig. 2d. The maximum and the statistical analysis of the absolute deviations for the two VOIs are summarized in Table 1.

3.2. Siemens Quantum

The Siemens Quantum gradient system is longer than the Sonata's and has a longer rise time and, therefore, the gradient field nonlinearity in this system is expected to be much less. This was confirmed by our measurement. The maximum absolute deviations measured in the Siemens Quantum system are shown in Fig. 3. Overall, the maximum absolute distortions are significantly less than on the Siemens Sonata. The maximum and mean absolute deviations for the two VOIs are summarized in Table 2. Within the cubic VOI, the maximum absolute deviations are ~4.0 mm or less and within the spherical VOI, the maximum absolute deviations are 2.5 mm or less. However, a close examination of Fig. 3a can reveal that the gradient linearity

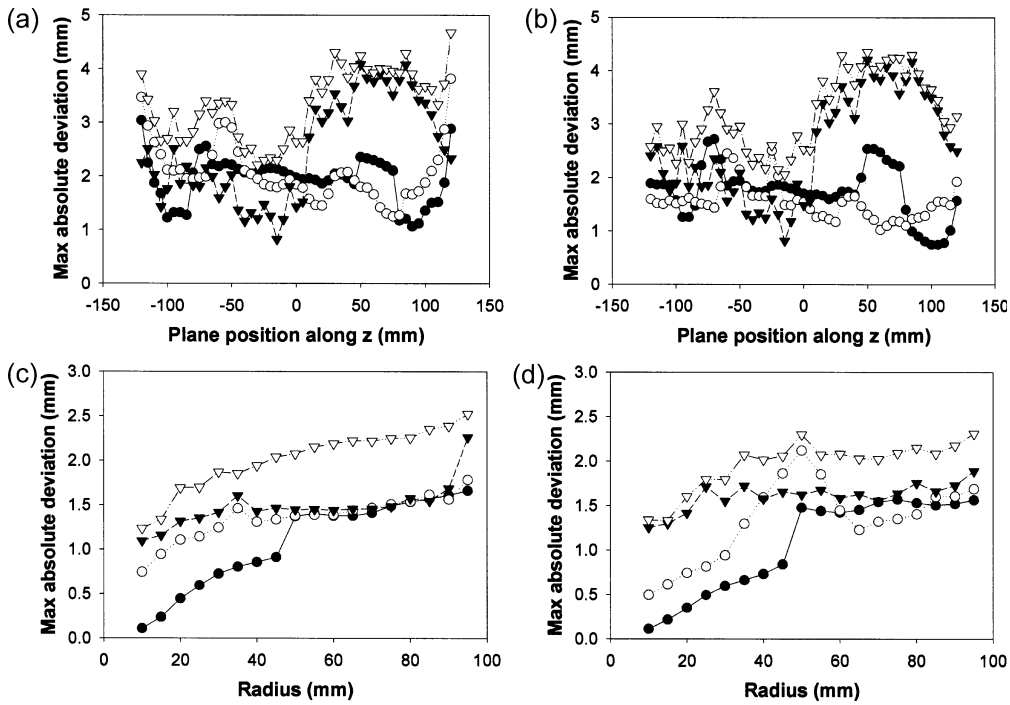

Fig. 3. The maximum absolute deviations (●, $|dx|_{max}$; ○, $|dy|_{max}$; ▼, $|dz|_{max}$;▽, dr_{max}) of the geometric distortion measured in a Siemens Quantum 1.5-T MRI system: (a) in axial planes on images acquired with no vendor's correction; (b) with vendor's correction applied in the xy plane; (c) on surface or spheres of different radius (no correction); (d) on surface of spheres of different radius (with correction).

Table 2
Summary of the statistical data (μ, σ, max) of the absolute deviations along x-, y- and z-axes and in the positional displacement (r) measured within a cubic VOI ($VOI_c(240)$: {(−120,120), (−120,120), (120,120)}) and a spherical VOI ($VOI_s(95)$: R=95 mm) in a 1.5-T Siemens Quantum system

VOI	Vendor's correction	Direction	μ (mm)	σ	max (mm)
$VOI_c(240)$	No	x	0.52	0.50	3.3
		y	0.63	0.45	3.8
		z	0.90	0.56	4.2
		r	1.38	0.57	4.8
	Yes	x	0.51	0.49	2.7
		y	0.52	0.36	2.5
		z	0.92	0.55	4.2
		r	1.33	0.54	4.4
$VOI_s(95)$	No	x	0.41	0.45	1.5
		y	0.50	0.35	1.8
		z	0.69	0.37	1.9
		r	1.09	0.42	2.3
	Yes	x	0.41	0.45	1.6
		y	0.45	0.30	2.1
		z	0.71	0.36	1.9
		r	1.07	0.40	2.3

in the X and Y gradients just begins to degenerate at the edges of the cubic VOI (at $z=\pm 120$ mm). Another noticeable difference exhibited by the Quantum system is that the vendor's correction method when applied in the xy plane made very little improvement [except at the edges of the VOI where the maximum absolute deviations ($|dx|_{max}$ and $|dy|_{max}$) were reduced to ~2.0 from 4.0 mm].

3.3. GE Signa EchoSpeed Plus BRM

For the X and Y gradients, the geometric distortion in this system showed very similar behavior to that for the Siemens Sonata system. The spatial characteristics of the geometric distortion with no correction are shown in Fig. 4a. The distortion along the x- and y-axes is relatively small in the central region of the magnet DSV ($|z|\leq 90$ mm), ~3 mm. The gradient field nonlinearity in the X and Y gradients becomes worse as $|z|$ increases from 90 mm. A significant feature of this gradient system is that the Z gradient shows exceptionally good linear behavior within the cubic VOI. The maximum absolute deviation dz_{max} was less than 2.0 mm for the entire cubic VOI. As shown in Fig. 4b, the small gradient nonlinearity of the Z gradient has made the 2D correction method applied in the xy plane extremely effective in terms of reducing the overall geometric distortion (dr). This was not the case for the Siemens Sonata system in which the gradient field nonlinearity of the Z gradient was significantly larger (see Fig. 2a). The maximum absolute deviations within the spherical VOI (VOIs(95)) before and after correction are shown, respectively, in Fig. 4c and d. The statistical and maximum absolute deviations within the two VOIs are summarized in Table 3.

3.4. GE Signa TwinSpeed TRM (Zoom)

Of the MRI systems investigated and for the two VOIs studied, this gradient set has the largest nonlinearity in the X and Y gradients and some unusual spatial characteristics were

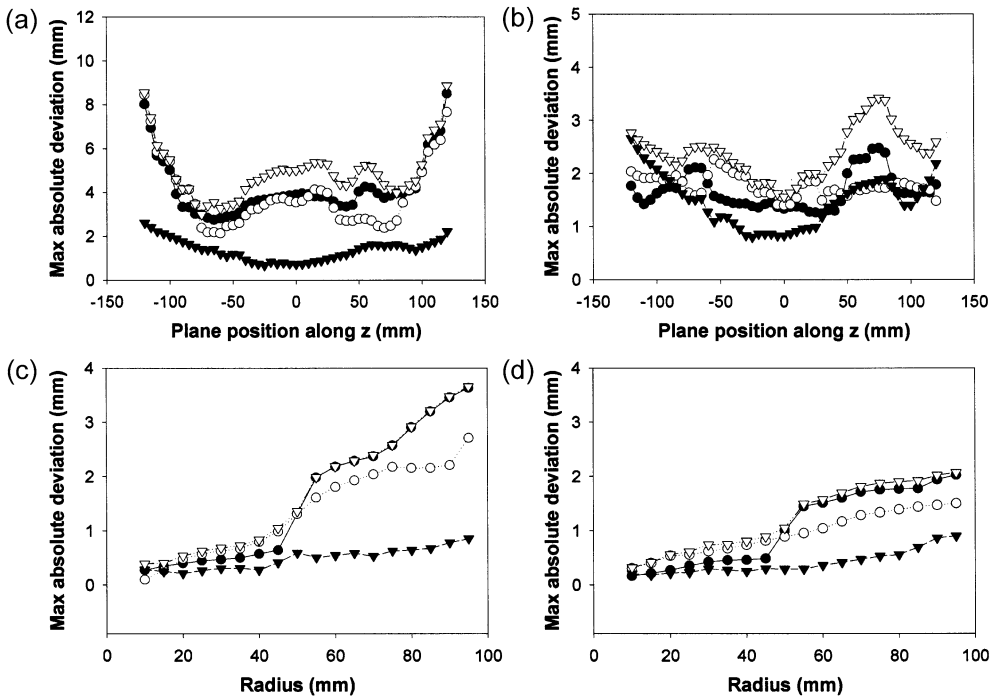

Fig. 4. The maximum absolute deviations (●, $|dx|_{max}$; ○, $|dy|_{max}$; ▼, $|dz|_{max}$;▽, dr_{max}) of the geometric distortion measured in a GE EchoSpeed Plus 1.5-T MRI system (BRM): (a) in axial planes on images acquired with no vendor's correction; (b) with vendor's correction applied in the xy plane; (c) on surface of spheres of different radius (no correction); (d) on surface of spheres of different radius (with correction).

Table 3
Summary of the statistical data (μ, σ, max) of the absolute deviations along x-, y- and z-axes and in the positional displacement (r) measured within a cubic VOI ($VOI_c(240)$: {(−120,120), (−95,120), (−120,120)}) and a spherical VOI ($VOI_s(95)$: $R=95$ mm) in a 1.5-T GE Signa EchoSpeed Plus system (BRM)

VOI	Vendor's correction	Direction	μ (mm)	σ	max (mm)
$VOI_c(240)$	No	x	1.56	1.50	8.5
		y	1.42	1.45	8.5
		z	0.35	0.32	2.6
		r	2.37	1.85	8.9
	Yes	x	0.63	0.50	2.5
		y	0.60	0.42	2.3
		z	0.39	0.34	2.7
		r	1.09	0.50	3.4
$VOI_s(95)$	No	x	0.57	0.58	3.6
		y	0.52	0.47	2.7
		z	0.17	0.13	0.9
		r	0.88	0.64	3.7
	Yes	x	0.47	0.42	2.0
		y	0.43	0.30	1.5
		z	0.17	0.14	0.9
		r	0.75	0.41	2.1

Table 4
Summary of the statistical data (μ, σ, max) of the absolute deviations along x-, y- and z-axes and in the positional displacement (r) measured within a cubic VOI ($VOI_c(240)$: {(−120,120), (−95,120), (−120,120)}) and a spherical VOI ($VOI_s(95)$: $R=95$ mm) in a 1.5-T GE TwinSpeed system (Zoom mode)

VOI	Vendor's correction	Direction	μ (mm)	σ	max (mm)
$VOI_c(240)$	No	x	4.45	4.56	25.1
		y	3.46	3.62	20.1
		z	1.07	1.24	9.7
		r	6.29	5.37	25.8
	Yes	x	0.76	0.51	3.8
		y	0.68	0.62	7.0
		z	1.08	1.23	9.7
		r	1.69	1.23	11.7
$VOI_s(95)$	No	x	1.30	1.15	6.4
		y	1.01	0.92	5.2
		z	0.30	0.23	1.2
		r	1.88	1.22	6.5
	Yes	x	0.59	0.43	2.1
		y	0.39	0.25	1.5
		z	0.28	0.22	1.1
		r	0.86	0.37	2.2

also observed. As shown in Fig. 5a (also see Table 4), the maximum absolute deviations along the x- and y-axes exceeded 20 mm in $VOI_c(240)$ and also showed some uncharacteristic behavior in spatial dependence. As shown in Fig. 5a in axial slices close to the isocenter, the maximum absolute deviation along the x- and y-axes ($|dx_{max}|$ and $|dy_{max}|$) first peaks at 18 and 14 mm, respectively. Then, the distortion decreases when moving away from the isocenter along both the +z and −z axes. For both the X and Y gradients it reaches a minimum of ~6 mm at $z=\sim\pm75$ mm. In more remote slices, the nonlinearity becomes worse again and increases more rapidly. Compared with the X and Y gradients,

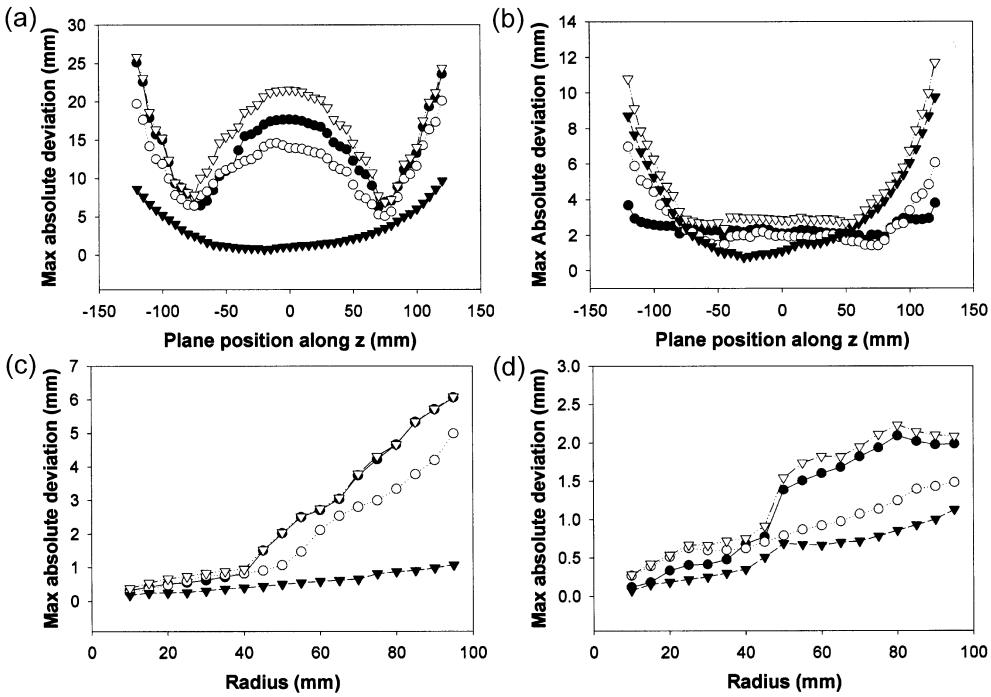

Fig. 5. The maximum absolute deviations (●, $|dx|_{max}$; ○, $|dy|_{max}$; ▼, $|dz|_{max}$;▽, dr_{max}) of the geometric distortion measured in a GE TwinSpeed 1.5-T MRI system (Zoom mode): (a) in axial planes on images acquired with no vendor's correction; (b) with vendor's correction applied in the xy plane; (c) on surface of spheres of different radius (no correction); (d) on surface of spheres of different radius (with correction).

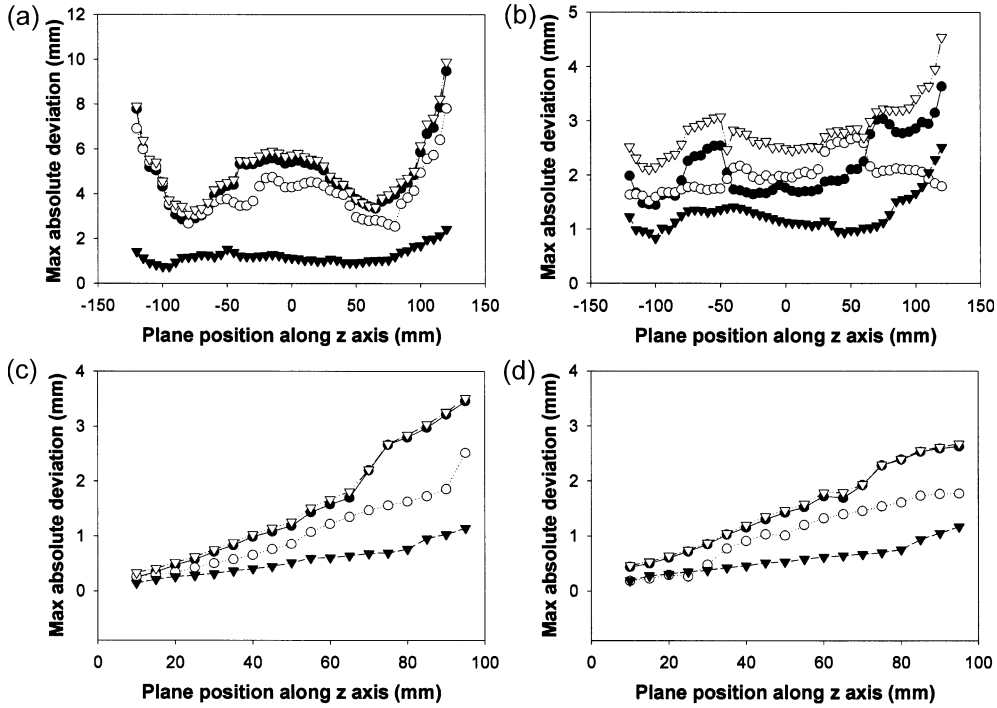

Fig. 6. The maximum absolute deviations (●, $|dx|_{max}$; ○, $|dy|_{max}$; ▼, $|dz|_{max}$;▽, dr_{max}) of the geometric distortion measured in a GE TwinSpeed 1.5-T MRI system (Whole mode): (a) in axial planes on images acquired with no vendor's correction: (b) with vendor's correction applied in the *xy* plane; (c) on surface of spheres of different radius (no correction); (d) on surface of spheres of different radius (with correction).

the nonlinearity in the *Z* gradient of this system is much less. The maximum absolute deviations along the *z*-axis are less than 10 mm within $VOI_c(240)$.

In Fig. 5b, the maximum absolute deviations measured with the vendor's correction method applied in the *xy* plane are presented (note that the vertical scale is different from that used in Fig. 5a). It is interesting to note that within the window $|z| \leq 75$ mm, the correction was effective with the maximum absolute deviations ($|dx_{max}|$ and $|dy_{max}|$) reduced to ~2 mm or less. However, in more remote slices ($|z| > 75$ mm), the correction became much less effective. At the $VOI_c(240)$ boundary of $|z| = 120$ mm, $|dx_{max}|$ is around 4 mm and $|dy_{max}|$ ~7 mm. It seems the correction method in the *xy* plane in this system has been optimized for the window of $|z| \leq 75$ mm. Within the spherical VOI, $VOI_s(95)$, the correction method applied in the *xy* plane is effective with the maximum absolute deviations all reduced to ~2.0 mm or less (see Fig. 5(d) and Table 4).

3.5. GE Signa TwinSpeed TRM (Whole)

The geometric distortion associated with this system is very similar to that found in GE's BRM gradient set. The maximum absolute deviations within the cubic VOI without and with vendor's correction are given in Fig. 6a and b, respectively, and that with the spherical VOI ($VOI_s(95)$) given in Fig. 6c and d. The statistical and maximum absolute deviations are summarized in Table 5.

In order to verify if the geometric distortion due to the static field inhomogeneity in the superconducting magnets equipped with modern shimming technologies is negligibly small, we have analyzed separately the geometric distortion in the Siemens Sonata system for contributions from the gradient field nonlinearity and that from the static field nonlinearity. The separation of these two different sources was made by using two sets of phantom images, one acquired with the readout (frequency encoding) direction

Table 5
Summary of the statistical data (μ, σ, max) of the absolute deviations along *x*-, *y*- and *z*-axes and in the positional displacement (r) measured within a cubic VOI ($VOI_c(240)$: {(−120,120), (−95,120) (−120,120)}) and a spherical VOI ($VOI_s(95)$: $R = 95$ mm) in a 1.5-T GE TwinSpeed system (Whole mode)

VOI	Vendor's correction	Direction	μ (mm)	σ	max (mm)
$VOI_c(240)$	No	*x*	1.64	1.51	9.5
		y	1.38	1.29	7.8
		z	0.44	0.35	2.4
		r	2.44	1.71	9.9
	Yes	*x*	0.97	0.67	3.6
		y	0.69	0.47	2.7
		z	0.46	0.36	2.5
		r	1.42	0.65	4.5
$VOI_s(95)$	No	*x*	0.77	0.60	3.5
		y	0.56	0.42	2.5
		z	0.27	0.21	1.1
		r	1.11	0.58	3.5
	Yes	*x*	0.81	0.57	2.6
		y	0.46	0.35	1.8
		z	0.29	0.22	1.2
		r	1.09	0.50	2.7

along the x-axis and the other with the readout along the y-axis [10]. The results showed that the geometric distortion that arises from the static field inhomogeneity was indeed negligibly small. The mean absolute geometric error was only 0.05 mm with a standard deviation of 0.14. As the time available for using the other clinical systems investigated in this study was limited, no such separate measurements were carried out for the other systems. However, we believe the static field ingomogeneity in the other systems should also be negligibly small. Therefore, the above-presented geometric distortion data included contributions from the gradient field nonlinearity and possibly from static field inhomogeneity, but the distortion from the latter source is negligibly small.

4. Discussion

Clearly, the problem of the gradient field nonlinearity in the new generation of high-speed gradient sets that employ short coils is much greater than in the previous generation of the gradient systems. Consequently, the geometric distortion caused by the gradient field nonlinearity in such gradient systems is much larger. As clearly shown in the present study, the magnitude of the gradient field nonlinearity varied considerably from system to system. If the maximum absolute deviations can be used as an indicator, the magnitude of the gradient field nonlinearity in the five gradient sets investigated differed approximately by five-fold. Within the cubic VOI of $240\times240\times240$ mm^3, the maximum absolute deviations in the MRI systems equipped with the gradient systems having fast rise times ranged between ~10 and 25 mm. In relative terms, these deviations represent geometric errors of ~8% to ~20%. By comparison, in the MRI systems equipped with gradient systems having much longer rise times, such as the Siemens Quantum system, the maximum absolute deviations fall in the range of 2–4 mm, corresponding to geometric errors of 2% to ~3%. Therefore, correction for geometric distortion due to the significantly large gradient field nonlinearity induced by the gradient systems when using gradient sets having a small length-to-diameter ratio is necessary.

Consequently, major MRI vendors such as GE and Siemens provide their customers with correction methods applied in 2D that have been integrated as part of the image postprocessing. The vendor's correction has made significant improvement especially for the GE's TRM Zoom system. For example, the maximum absolute deviation along the x-axis within $\mathrm{VOI_c}(240)$ was reduced from 25.1 to 3.8 mm (see Table 4). It should be pointed out, however, that if the correction were applied in the xz or yz plane, the effectiveness of the correction would be significantly reduced as the gradient field nonlinearity along the normal to the correction plane in these two cases, in the Y and X gradients, respectively, is much greater than in the Z gradient.

As stated, the current correction methods offered by both GE and Siemens are 2D methods. The reason for this was probably that correction for geometric distortion in 2D was the only possible method for correcting geometric distortion in a single slice or in multiple noncontiguous slices. In principle, use of a 2D method to correct geometric distortion in MRI is an incomplete approach and it can only be expected to work well when the geometric distortion along the normal of the correction plane is small. If the geometric distortion along the normal of the imaging plane is large, correction in 2D (within the imaging plane) offers only an approximation and its value can be significantly reduced. This point can be better appreciated in image-based spatial localization used in stereotactic radiosurgery or radiotherapy. In such applications, the geometric errors in the displacement vector, dr, matters most. In order to determine dr, clearly, geometric errors along all three orthogonal directions (dx, dy, dz) need to be measured. When employing high-speed gradient sets, the representative cases have demonstrated the limitation of the 2D correction methods. For example, as shown in Table 1, the 2D correction applied in xy plane reduced the distortion along the x- and y-axes from more than 10 to around 3.0 mm, but the maximum absolute distortion $\mathrm{d}r_{\max}$ was reduced only marginally, from 11.4 to 9.6 mm. Therefore, any correction made in 2D requires care in the interpretation and application as the true nature of the geometric distortion in MRI is 3D.

For neuro-imaging applications of MRI, geometric distortion is a particularly concerning issue. The comprehensive assessment carried out in the present study for the spherical VOI, $\mathrm{VOI_s}(95)$, should provide useful information of when care needs to be exercised for neuro-imaging applications. The results suggest that the gradient systems designed for MRI are generally optimized to have the most linear regions around the system's isocenter. For example, in the GE TRM Zoom system, the maximum absolute deviations within $\mathrm{VOI_c}(240)$ exceeded 25 mm whereas in $\mathrm{VOI_s}(95)$, they were ~6.0 mm or less (see Table 4). A more satisfactory finding in the present study is that with the vendor's correction applied in the xy plane, the maximum absolute deviations within $\mathrm{VOI_s}(95)$ are all below ~2.5 mm (see Tables 1–5). It can be concluded that for neuro-imaging applications with the imaging object optimally positioned at the isocenter and the 2D correction method applied in the xy plane, the maximum absolute deviations in the investigated MRI systems can be minimized to be around 2 mm or less. Whether such a degree of accuracy is sufficient is a clinical decision.

The geometric distortion in the MRI systems studied does, however, increase significantly in areas more remote from the system's isocenter and this is clearly shown in the results for the high-speed gradient systems (see Figs. 2a and 5a). For example, the rate of change in $\mathrm{d}r_{\max}$ along the z-axis ($\mathrm{d}r_{\max}/z$) at the boundaries of $\mathrm{VOI_c}(240)$ ($z=\pm120$ mm) was ~0.6 for GE TRM Zoom and ~0.4 for Siemens Sonata. In other words, for every 5 mm further away from the isocenter along the z-axis, $\mathrm{d}r_{\max}$ would increase 3 and 2 mm,

respectively, in these two systems. It is advisable that MRI users should be aware that for imaging peripheral areas, significantly large geometric distortions can be present.

It is important to note that the use of the positional deviations to characterize the geometric distortion as adopted in the present study is slightly different from that recommended by AAMP [9] and by The Institute of Physics and Engineering in Medicine (United Kingdom, [19]). In these recommended methods, the geometric distortion in MRI is measured by the difference in distance between a pair of points measured in the distorted image space and the true distance between them. This measurement procedure has a disadvantage in that the points used are not well defined. In using the positional deviations, however, the distortion is uniquely defined by a point's true position and its displaced position in the distorted image space. Therefore, the distortion characterized in this way offers a common platform on which a standard procedure for assessing the geometric distortion in MRI can be developed.

The detailed geometric distortion data gathered in the present study also show some indications of the limitation of the vendor's correction methods. Firstly, for correcting large geometric distortions present in gradient systems having a short rise time, the effectiveness of the correction varied considerably and became much less effective in slices further away from the system's isocenter. This has been shown for both the GE TRM Zoom and Siemens Sonata systems. Secondly, there appears to be an ultimate limitation on how much improvement the vendor's correction methods could achieve. With the correction methods applied in the *xy* plane, the maximum absolute deviations measured in the "residual" distortion in the corrected phantom images were still relatively large, between ~2.0 and 7.0 mm within a volume of $240\times240\times240$ mm^3. Thirdly, the data on the Quantum system presents an interesting case. For this system, the vendor's correction method did not appear to have made any noticeable improvement on correcting the geometric distortion. On the other hand, the geometric distortion in this system is overall the smallest with the maximum absolute distortions of ~4 mm or less. The observation of virtually no improvement in this particular case may indicate that the ultimate improvement the vendor's correction could achieve had been reached.

It is rather difficult to speculate on the factors that affected the ultimate performance of the vendor's correction methods as the details of these methods were not known to us. However, the recent studies on the possible effects of gradient field nonlinearity in MRI [2,4] may suggest the vendor's correction methods involve the use of a spherical harmonics expansion to approximate the magnetic fields generated by the gradient coils [20,21]. If this is the case, there are a number of possible sources that could contribute to errors that may ultimately impose some limitations on the effectiveness of the correction. Firstly, the use of spherical harmonics expansion can suffer from a truncation effect as only a limited number of terms might have been included in the actual implementation of a spherical harmonics expansion. Secondly, the use of the magnetic fields either calculated from the coils geometry or derived from the calibration settings (normally obtained at the time of installation or during the last major service) clearly does not take into account any temporal variability of the gradients during use. It does not appear to be appreciated that the noise that arises from gradient pulsing is due to wire movement and there may well be a long-term temporal variation in the nonlinearity. Thirdly, a possible violation of the quasi-static approximation of the current distribution model can also lead to some errors [20].

The recently developed phantom-based technique that was used in the present study can overcome these shortfalls. In particular, provision of a comprehensive spatial mapping of the geometric distortion allows the correction to be made using more desirable methods such as splines. With the possibility of using piecewise interpolation methods, the spatial variability of the geometric distortion can be modeled in a more satisfactory manner. This has been demonstrated in the following paper (Part II) where the results using a new correction method [8] based on the phantom-mapped geometric distortion data are presented and discussed.

5. Conclusions

Assessment of the geometric distortion in a range of clinical 1.5-T MRI systems has been carried out using a new 3D phantom-based technique. This work represents the most comprehensive assessment of the geometric distortion in MRI systems to date. Among the investigated systems, the geometric distortion is much larger in gradient systems in which short coils are used. By comparison, geometric distortion in the gradient systems having a larger length to diameter ratio is much less. The geometric distortion data obtainable with this technique as illustrated in this paper on four representative MRI systems offer unprecedented details encompassing both the overall and spatial characteristics of the geometric distortion. The detailed analysis of the geometric distortion within a cubic VOI and a spherical VOI should provide more useful and specific information in relation to body- and neuro-imaging applications. In addition, the effectiveness of the vendor's 2D correction methods has been thoroughly and quantitatively investigated. While these methods can make significant improvements in the correction of the considerably large geometric distortion found in high-speed gradient systems, their limitations are also clearly demonstrated in the present study. For example, for the Siemens Quantum system which showed the least geometric distortion, there was no noticeable improvement overall with the vendor's correction method. In addition, these correction methods appear to have been optimized for a volume around the isocenter. The data gathered in the present study suggest that the effectiveness of the correction by these methods falls rapidly in more remote areas (see Fig. 5b in particular).

Therefore, the limitations and some shortfalls associated with these 2D correction methods cannot be overlooked.

Acknowledgment

We thank the staff at our workshop for their excellent work in the construction of the 3D phantom.

References

[1] Bammer R, Markl M, Pelc NJ, Moseley ME. Assessment of spatial gradient field distortion in diffusion-weighted imaging. Proc. of 10th annual meeting of ISMRM, Honolulu; 2002. p. 1172.

[2] Bammer R, Markl M, Barnett A, et al. Analysis and generalized correction of the effect of spatial gradient field distortions in diffusion-weighted imaging. Magn Reson Med 2003;50:560–9.

[3] Markl M, Draney MT, Pelc NJ. Analysis and correction of the effect of spatial gradient field distortion on velocity measurements with phase contrast MRI. Proc. of 10th annual meeting of ISMRM, Honolulu; 2002. p. 381.

[4] Markl M, Bammer R, Alley MT, et al. Generalized reconstruction of phase contrast MRI: analysis and correction of the effect of gradient field distortions. Magn Reson Med 2003;50:791–801.

[5] Wang DM, Rose S, de Zubicaray G, et al. Improving the speed of assessment of magnetic resonance imaging measures of the progress of Alzheimer's disease, 12-month longitudinal studies feasible? Neurobiol Aging 2002;23:1543.

[6] Wang DM, Chalk JB, Rose S, et al. Global and regional rates of brain atrophy in Alzheimer's disease using structural MRI. Clin Neuropsychol Assess 2000;1:26–7 [Special Issue].

[7] Wang DM, Chalk JB, Rose S, et al. MR image-based measurement of rates of change in volumes of brain structures Part II: application to a study of Alzheimer's disease and normal aging. Magn Reson Imaging 2002;20:41–8.

[8] Wang DM, Doddrell DM, Cowin G. A novel phantom and method for comprehensive 3-dimensional measurement and correction of geometric distortion in magnetic resonance imaging. Magn Reson Imaging 2004;22:529–42.

[9] Price RR, Axel L, Morgan T, Newman R, Perman W, Schneiders N, et al. Quality assurance methods and phantoms for magnetic resonance imaging: report of AAPM nuclear magnetic resonance task group no. 1. Med Phys 1990;17:287–95.

[10] Kawanaka A, Takagi M. Estimation of static magnetic field and gradient fields from NMR image. J Phys E: Sci Instrum 1986;19:871–5.

[11] Mizowaki T, Nagata Y, Okajima K, et al. Reproducibility of geometric distortion in magnetic resonance imaging based on phantom studies. Radiother Oncol 2000;57:237–42.

[12] Walton L, Hampshire A, Forster DMC, Kemeny AA. A phantom study to assess the accuracy of stereotactic localization, using T1-weighted magnetic resonance imaging with the Leksell stereotactic system. Neurosurgery 1996;38:170–8.

[13] Yu C, Apuzzo MLJ, Zee CS, Petrovich Z. A phantom study of the geometric accuracy of computed tomographic and magnetic resonance imaging stereostatic localization with the Leksell stereostatic system. Neurosurgery 2001;48:1092–9.

[14] Orth RC, Sinha P, Madsen EL, et al. Development of a unique phantom to assess the geometric accuracy of magnetic resonance imaging for stereotactic localization. Neurosurgery 1999;45:1423–31.

[15] McRobbie DW. A three-dimensional volumetric test object for geometric evaluation in magnetic resonance imaging. Med Phys 1997;24:737–42.

[16] Mah D, Stechner M, Palacio E, et al. Characteristics and quality assurance of a dedicated open 0.23 R MRI for radiation therapy simulation. Med Phys 2002;29:2541–7.

[17] Wang DM, Doddrell DM. A proposed scheme for comprehensive characterization of geometric distortion measured using a 3-dimensional phantom in magnetic resonance imaging. Med Phys 2004;31:2212–18.

[18] Sonka M, Hlavac V, Boyle R. Image processing, analysis and machine vision. International Thomson Publishing Inc.;1996.

[19] Lerski RA, de Wilde J, Boyce D, Ridgeway J. Quality control in magnetic resonance imaging. IPEM Report 80. York: The Institute of Physics and Engineering in Medicine; 1998.

[20] Romeo F, Hoult DI. Magnet field profiling: analysis and correcting coil design. Magn Reson Med 1984;1:44–65.

[21] Glover GH, Pelc NJ. Method for correcting image distortions due to gradient nonuniformity. US Patent 4,591,789; 1986.